

Topology-Aware Block Coordinate Descent for Qubit Frequency Calibration of Superconducting Quantum processors

Zheng Zhao,^{1,2} Weifeng Zhuang,³ Yanwu Gu,³ Peng Qian,³ Xiao Xiao,³ and Dong E. Liu^{1,2,3,4,*}

¹*State Key Laboratory of Low Dimensional Quantum Physics,*

Department of Physics, Tsinghua University, Beijing, 100084, China

²*Frontier Science Center for Quantum Information, Beijing 100184, China*

³*Beijing Academy of Quantum Information Sciences, Beijing 100193, China*

⁴*Hefei National Laboratory, Hefei 230088, China*

Pre-execution calibration is a major bottleneck for operating superconducting quantum processors, and qubit frequency allocation is especially challenging due to crosstalk-coupled objectives. We establish that the widely-used Snake optimizer is mathematically equivalent to Block Coordinate Descent (BCD), providing a rigorous theoretical foundation for this calibration strategy. Building on this formalization, we present a topology-aware block ordering obtained by casting order selection as a Sequence-Dependent Traveling Salesman Problem (SD-TSP) and solving it efficiently with a nearest-neighbor heuristic. The SD-TSP cost reflects how a given block choice expands the reduced-circuit footprint required to evaluate the block-local objective, enabling orders that minimize per-epoch evaluation time. Under local crosstalk/bounded-degree assumptions, the method achieves linear complexity in qubit count per epoch, while retaining calibration quality. We formalize the calibration objective, clarify when reduced experiments are equivalent or approximate to the full objective, and analyze convergence of the resulting inexact BCD with noisy measurements. Simulations on multi-qubit models show that the proposed BCD-NNA ordering attains the same optimization accuracy at markedly lower runtime than graph-based heuristics (BFS, DFS) and random orders, and is robust to measurement noise and tolerant to moderate non-local crosstalk. These results provide a scalable, implementation-ready workflow for frequency calibration on NISQ-era processors.

I. INTRODUCTION

Quantum computing is widely regarded as a transformative technology with the potential to solve problems that are intractable for classical computers, such as quantum chemistry, combinatorial optimization, and cryptography [1–10]. Among the leading platforms for quantum computing, superconducting circuits have demonstrated significant progress toward building scalable, high-fidelity quantum processors[11–18]. However, the current state of quantum computing remains in the Noisy Intermediate-Scale Quantum (NISQ) era [19, 20], where quantum systems are characterized by limited qubit numbers and significant noise. In this context, developing effective calibration strategies to achieve high-fidelity quantum operations is critical for advancing practical quantum computing.

However, as the number of qubits in a quantum processor increases, the calibration of system parameters becomes a challenging task[21, 22]. The entanglement in quantum systems and the potential crosstalk between control parameters result in an exponential growth in the search space for optimization, leading to the difficult in identifying optimal or local optimal within a reasonable time frame. Furthermore, the complexity of quantum circuits used for calibration grows exponentially with the number of qubits, further complicating the optimization process. Therefore, efficient multi-parameter optimization algorithms are essential to ensure the calibration of large-scale quantum systems within practical constraints.

Among the various parameters requiring calibration[11, 23–34], frequencies of qubit play a significant role in determining the fidelity of superconducting quantum circuits [35–38]. Frequency control impacts not only individual qubit performance but also the mitigation of crosstalk between qubits, which is critical for achieving high-fidelity quantum gates [39–41]. Previous studies have attempted to address frequency allocation problems using artificial intelligence techniques [42] or optimization methods, such as the Snake optimizer [15, 43]. The Snake optimizer, while presented as a graph-traversal-based calibration strategy, is fundamentally an instance of the Block Coordinate Descent (BCD) algorithm applied to quantum processor calibration. In this work, we make this connection explicit by establishing the mathematical equivalence between Snake and BCD, providing a rigorous theoretical framework that enables the application of classical optimization theory to quantum processor calibration. This formalization reveals that the block traversal order—treated as a heuristic choice in the original Snake proposal—is a key degree of freedom that

* Corresponding to: dongeliu@mail.tsinghua.edu.cn

can be systematically optimized. Other multi-parameter optimization algorithms have also been explored [44–52], but these methods often suffer from long optimization times or difficulties in convergence when applied to complex quantum systems, highlighting the need for more efficient and scalable strategies.

In this work, we propose an enhanced optimization framework that combines the Block Coordinate Descent (BCD) algorithm with the Nearest Neighbor Algorithm (NNA) to tackle the frequency allocation problem in quantum processor calibration. Our approach leverages the topology of quantum chips and crosstalk structure to significantly reduce optimization complexity while maintaining accuracy. The contributions of this study are as follows:

1. We establish the mathematical equivalence between the Snake optimizer [15, 43] and Block Coordinate Descent (BCD), providing a rigorous theoretical foundation for this widely-used calibration strategy and enabling the application of classical optimization theory to quantum processor calibration.
2. We formulate the block ordering problem as a Sequence-Dependent Traveling Salesman Problem (SD-TSP) and solve it efficiently using the Nearest Neighbor Algorithm (NNA). This principled approach yields systematic complexity reduction compared to the graph-based heuristics (BFS, DFS) employed in the original Snake implementation.
3. We provide a rigorous complexity analysis demonstrating $\mathcal{O}(N)$ scaling under local crosstalk assumptions. We further characterize the benefits of ordering optimization under two complexity models: an empirical model reflecting practical implementations, and the search-space model from Ref. [43] representing theoretical worst-case complexity.
4. Through extensive numerical simulations, we validate the convergence, efficiency, and robustness of the proposed algorithm under measurement noise and non-local crosstalk conditions.

This study offers a new perspective on calibration strategies for NISQ-era quantum processors, paving the way for more efficient and scalable approaches to enhance quantum system performance.

II. RESULTS

Our methodology for calibrating qubit frequencies addresses the challenge of exponential complexity by decomposing the global optimization problem. This approach begins by leveraging preliminary characterization data, including the processor’s physical topology and a map of its crosstalk interactions, to partition the system’s parameters into manageable blocks. For each block, we then define a local objective function evaluated through a reduced-scale calibration experiment. The guiding principle is to construct this experiment using the minimum number of qubits necessary to capture the full impact of the parameters within the block, including all significant crosstalk effects. This “crosstalk footprint” is determined from prior knowledge of the system; for example, a local crosstalk model assumes interactions are confined to physically adjacent qubits, whereas a more complex model might account for non-local couplings.

By restricting the calibration experiment to this minimal qubit footprint, we ensure the objective function remains computationally tractable, as its evaluation complexity typically scales exponentially with the number of qubits involved. While recent work [15, 42] has demonstrated the use of machine learning to generate surrogate objective functions from experimental data, our strategy of defining a reduced objective based on a physical crosstalk model is a complementary and vital technique for managing complexity. Even when a global objective function is learned, its evaluation for a local parameter update can be made vastly more efficient by considering only the terms relevant to that block’s crosstalk footprint.

This framework of sequential, block-wise optimization is implemented using the Block Coordinate Descent (BCD) algorithm. The overall efficiency of this process is critically dependent on the strategy used to partition parameters into blocks and the sequence in which these blocks are optimized. An effective blocking and ordering strategy, as we will detail, minimizes the computational cost per calibration epoch, enabling the efficient enhancement of quantum circuit fidelity.

A. The role of crosstalk in defining local calibration

The central challenge in calibrating a specific block of parameters, denoted as B , is that adjustments can have unintended consequences on other parts of the quantum circuit. This phenomenon, known as crosstalk, arises from unwanted physical interactions, such as parasitic flux coupling or residual ZZ interactions between qubits. To manage

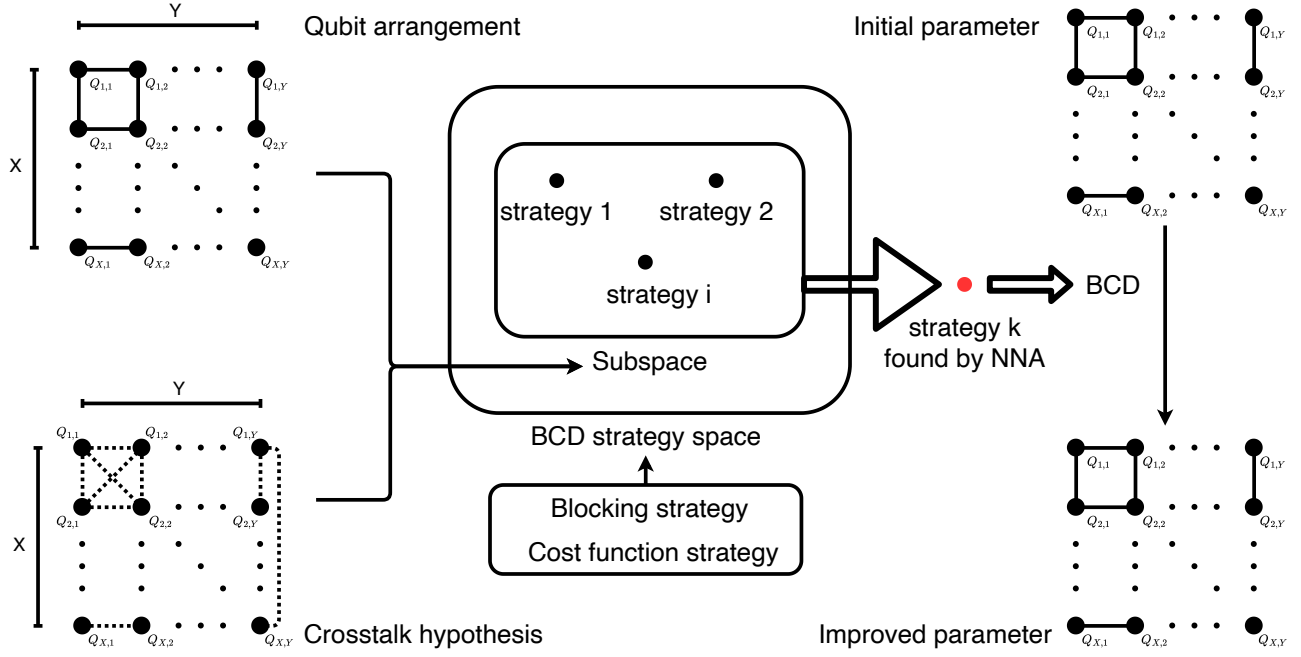


FIG. 1. Flowchart of algorithm and results. Arrangement of qubits and crosstalk hypothesis are sent to the Block coordinate descent(BCD) algorithm. How to block parameters and how to determine the reduced cost function are defined in this algorithm, then the complexity of BCD algorithm can be determined. With nearest-neighbor algorithm(NNA) for sequence-dependent traveling salesman problem(TSP), a optimized strategy with less complexity is found. Parameters leading to higher fidelity will be chosen by BCD algorithm. Due to the different relationship between crosstalk hypothesis and actual crosstalk, the fidelity may increase strictly or non-strictly.

this complexity, our block coordinate descent approach relies on a local calibration experiment, G' , designed to be computationally tractable while accurately capturing the effects of varying the parameters in B .

For this local experiment to be valid, its optimization landscape must be consistent with that of the full, global calibration experiment, G . Formally, G' preserve the ordering induced by G when all other parameters are held constant. This validity condition is expressed as:

$$G'(B|f \setminus B) = h(G(B|f \setminus B)) \quad (1)$$

where the function h is strictly increasing, B represents one block of parameters in chip and f represents the set of all parameters. This condition ensures that a step taken to optimize the local experiment does not contradict the objective of the global optimization.

The validity of the inclusion condition in Eq. (1) depends entirely on the construction of the local experiment G' . Specifically, G' must incorporate all gates whose performance is affected by the parameters in block B . Identifying this set of gates requires an underlying crosstalk model, a set of assumptions about which components in the system interact. Two principal approaches exist for defining this model.

The first approach is to use an exhaustive model, which assumes all-to-all connectivity. This defines an inclusion range for G' that encompasses every qubit in the processor. Such a comprehensive construction guarantees that all crosstalk effects are captured, ensuring the validity of Eq. (1) by definition. While theoretically sound, this method is only practical for very small quantum systems, as the experimental and computational complexity scales intractably with the number of qubits. For larger systems, its value is primarily theoretical, confirming that a valid experiment G' always exists.

The second, more practical approach is to employ a heuristic model. This model is typically based on physical priors, such as the chip's known connectivity graph (e.g., nearest-neighbor coupling), and is refined with data from preliminary characterization experiments. This leads to a tractable experiment G' with a limited scope. However, this strategy introduces the critical risk of a model-reality mismatch. If the heuristic model is an incomplete or inaccurate representation of the true physical crosstalk, then the experiment G' will fail to account for all relevant interactions. Consequently, the inclusion condition in Eq. (1) may be violated, causing the local optimization to converge towards

a solution that is suboptimal for the global system. The iterative process of detecting further crosstalk and expanding the experiment's scope corresponds to an attempt to refine this heuristic model until the validity condition is met.

When employing a heuristic model, the iterative process of refining it to account for physical crosstalk can lead to intermediate stages where a model-reality mismatch persists. In these scenarios, the inclusion condition in Eq. 1 is only approximately satisfied, indicating that the local optimization may converge to a suboptimal solution for the global system. The optimization algorithm can then proceed via one of two adaptive strategies:

1. Continue the iterative refinement of the heuristic model. This involves detecting further crosstalk effects and expanding the experiment's scope (G') until the inclusion condition in Eq. 1 is rigorously met.
2. Halt the refinement process and proceed with the optimization using the current, tractable heuristic model. This approach accepts the existing model-reality mismatch in exchange for avoiding the increased experimental and computational burden of further model expansion.

The choice between these strategies represents a critical trade-off between the accuracy of the final optimized solution and the practical costs of characterization.

B. Block coordinate descent algorithm

This section details the optimization framework for calibrating the device parameters, which we formulate as the following problem:

$$\min_{f_i \in \mathcal{F}_i} G(f_1, f_2, \dots, f_N) \quad (2)$$

Here, $\mathbf{f} = (f_1, f_2, \dots, f_N)$ is the vector of tunable device parameters, such as qubit frequencies, confined to a feasible set $\mathcal{F} = \prod_{i=1}^N \mathcal{F}_i$, where each $\mathcal{F}_i \subseteq \mathbb{R}$ is a closed, convex set. The objective function $G : \mathcal{F} \rightarrow \mathbb{R}$ is a continuous function that quantifies the calibration experiments of the quantum device. Crucially, $G(\mathbf{f})$ is not an analytical expression but a value estimated from the outcomes of physical calibration experiments, which are subject to inherent experimental noise.

The experimental nature of evaluating $G(\mathbf{f})$ makes gradient-based optimization methods impractical. Estimating the partial derivative $\frac{\partial G}{\partial f_i}$ using methods like finite differences would require numerous high-precision experiments for each parameter, rendering the process prohibitively slow and resource-intensive. This challenge motivates our use of a derivative-free optimization strategy. Specifically, we employ a Block Coordinate Descent (BCD) algorithm, which iteratively optimizes the system by solving smaller, more manageable subproblems.

To exploit the problem's structure, we partition the parameters into M (possibly overlapping) blocks $\mathcal{B} = \{B_j\}_{j=1}^M$, where $\cup_j B_j = (f_1, f_2, \dots, f_N)$. In each step of our Block Coordinate Descent (BCD) algorithm, we solve a subproblem focused on a single block B_j . This subproblem is formulated as:

$$\min_{f_{j_i} \in \mathcal{F}_{j_i}} G_{B_j}(f_{j_1}, f_{j_2}, \dots) \quad (3)$$

where the minimization is performed over all parameters $\{f_{j_i}\}$ that constitute the block B_j . The cost function G_{B_j} is defined based on a heuristic experimental model, G' , as:

$$G_{B_j}(u) := G'(u, \setminus B_j) \quad (4)$$

In this definition, u represents the set of parameters within block B_j , while $\setminus B_j$ represents the complementary set of parameters held constant during the subproblem optimization. The function $G' : \Pi_{i=1}^N \mathcal{F}_i \rightarrow \mathbb{R}$ represents the value measured from a specific calibration experiment. The ideal choice, $G' = G$, would require a full-chip experiment for every subproblem, which is computationally prohibitive as the number of qubits increases. Therefore, by assuming that crosstalk effects are primarily local, we can adopt a more prudent approach: we define and select a tractable G' that models a smaller, localized experiment sufficient for optimizing the parameters in block B_j .

A single iteration of the Block Coordinate Descent (BCD) algorithm involves selecting one block B_j from the set of blocks \mathcal{B} and solving the corresponding optimization subproblem. This subproblem aims to find the optimal parameters for the selected block, denoted B_j^* , by minimizing the local heuristic objective function G_{B_j} :

$$B_j^* \in \arg \min_{B_j} G_{B_j}(B_j) \quad (5)$$

In this expression, the minimization $\arg \min_{B_j}$ is performed with respect to the set of parameters contained within block B_j , while all other parameters outside this block are held constant. After finding a solution vector $B_j^* =$

$(f_{j_1}^*, f_{j_2}^*, \dots)$, the global parameter vector $f = (f_1, f_2, \dots, f_N)$ is updated by replacing the parameters in B_j with their new values from B_j^* . A complete pass through all blocks in \mathcal{B} constitutes one epoch of the algorithm. The full pseudocode for this procedure is presented in Alg. 1.

Algorithm 1 Block Coordinate Descent

Require: $f^{0,0}$ starting point; \mathcal{F} parameter space; $\{B_1, B_2, \dots, B_M\}$ blocks of parameters; G overall cost function; $\{G_1, G_2, \dots, G_M\}$ sub-cost functions

Ensure: G^* , the convergence value of G

- 1: set epoch $j \leftarrow 0$
- 2: **repeat**
- 3: $j \leftarrow j + 1$
- 4: set $f^{j,0} \leftarrow f^{j-1,k}$
- 5: set step $k \leftarrow 0$
- 6: **repeat**
- 7: $k \leftarrow k + 1$
- 8: choose $j_k \in \{1, 2, \dots, M\}$ to determine block B_{j_k}
- 9: choose $B_{j_k}^{j,k} \in \arg \min_{B_{j_k}} G_{B_{j_k}}(B_{j_k} \mid f^{j,k-1} \setminus B_{j_k}^{j,k-1})$
- 10: $f^{j,k} \leftarrow (B_{j_k}^{j,k}, f^{j,k-1} \setminus B_{j_k}^{j,k-1})$
- 11: **until** each parameter is optimized at least once
- 12: **until** convergence

There are three key components in implementing the BCD algorithm: the block strategy, how to select block each step, and how to optimize each subproblem.

For the block strategy, since we know the spatial distribution of qubits on superconducting quantum chips, we typically group spatially neighboring parameters together. Under the assumption of local crosstalk, the influence ranges of parameters within this block overlap. This implies that for a fixed number of parameters in a block, the influence range is minimized. A minimized influence range means we can more easily obtain the objective function value through calibration experiments. Therefore, this paper employs a non-overlapping block strategy centered around each qubit to narrow the search space for partitioning. Section II F explores more suitable partitioning strategies within this space. Clearly, another parallel partitioning strategy space exists. When parameters within each grouping are spaced as far apart as possible in the parameter space, their influence ranges become mutually independent due to the assumption of local crosstalk. In this case, optimizing parameters independently within each region significantly reduces both the search space and the complexity of the objective function. However, this scenario is uncommon in the NISQ stage with fewer qubits and is therefore not discussed in detail in this paper.

For each block selection, the BCD algorithm can either adopt a fixed selection order and iterate, or choose based on certain rules each time. For instance, selecting the block direction that maximizes the reduction in the objective function is a common approach in the BCD algorithm. However, this can lead to issues in chip calibration problems, specifically the aforementioned difficulty in differentiation for this problem. Therefore, selecting a fixed order is a viable option for chip calibration problems. Furthermore, by fixing the optimization problem to be solved at each epoch, we can determine the computational complexity of the optimization algorithm at each step. This insight guides us toward developing more effective block strategies.

Finally, we address the optimization problem for the subproblems. Here, we have significantly reduced the dimensionality of the search space, making the choice of optimization algorithms relatively arbitrary. The only requirement is that each optimization algorithm provides its computational complexity so that the overall complexity of each epoch of the BCD algorithm can be calculated. Here we present a method below.

Solving the subproblem in Eq. (5) is itself a multi-parameter optimization challenge of dimension $|B_j|$, which must be addressed without access to analytical gradients. To this end, we employ an iterative local search algorithm. Starting from the current parameters for the block, B_j^0 , the method generates a sequence of updates $B_j^{t+1} = B_j^t + d_t r_n$. The step size r_n is set according to the main BCD epoch number n ; inspired by the stochastic approximation literature [53], we use the diminishing step size $r_n = \frac{1}{n}$. The direction vector d_t is determined at each sub-iteration by performing a search over a discrete set of local directions:

$$d_t = \arg \min_{d \in S} G_{B_j}(B_j + dr_n) \quad (6)$$

The search space S is the set of all vectors whose components are restricted to $\{-1, 0, 1\}$:

$$S = \{\mathbf{v} \mid v_i \in \{-1, 0, 1\}, \forall i \in \{1, 2, \dots, |B_j|\}\}. \quad (7)$$

This procedure effectively evaluates the objective function at all $3^{|B_j|}$ points on a hypergrid centered at B_j^t . If a candidate point $B_j^t + dr_n$ lies outside the feasible domain where G_{B_j} is defined, it is excluded from the minimization. Since the zero vector is included in S , this process guarantees that the objective function is non-increasing, as $G_{B_j}(B_j^{t+1}) \leq G_{B_j}(B_j^t)$.

The primary cost of this procedure is the number of physical experiments required. We can quantify the experimental complexity for optimizing block B_j as:

$$\mathcal{T}(B_j) = S_j \times T(G_{B_j}) \quad (8)$$

Here, $T(G_{B_j})$ represents the cost (e.g., time) of performing a single experiment to evaluate the local objective function G_{B_j} , and S_j is the total number of such evaluations needed to solve the subproblem. This number of evaluations is determined by:

$$S_j = S \times 3^{|B_j|} \quad (9)$$

In this expression, $3^{|B_j|}$ is the size of the search-direction set S defined previously. The variable S in this specific context denotes the number of iterations performed by the iterative search in Eq. (6) to converge to a solution for the block.

C. Convergence of BCD Algorithm

This section analyzes the convergence properties of the BCD algorithm under the conditions relevant to quantum device calibration. We begin by establishing convergence in an idealized theoretical setting before examining how practical factors like inexact optimization, measurement noise, and model mismatch affect performance. To demonstrate convergence, we first make several standard assumptions about the objective function and the parameter space. Under these conditions, we can guarantee that the value of the objective function converges.

Assumption 1. (Regularity)

- The global objective function $G : \Pi_{i=1}^N \mathcal{F}_i \rightarrow \mathbb{R}$ is proper, lower bounded, and continuously differentiable on an open set containing $\Pi_{i=1}^N \mathcal{F}_i$.
- Each parameter space $F_i \subseteq \mathbb{R}$ is a closed, convex set.

Assumption 2. (Physical condition)

- (Local crosstalk) For any block $B_j \in \mathcal{B}$, a local objective function G_{B_j} can be defined such that its evaluation complexity $T(G_{B_j})$ is independent of the total number of qubits N .
- (Equivalence) The local objective function G_{B_j} is a valid surrogate function for the global objective function G , meaning G_{B_j} preserves the ordering induced by G when all other parameters are held constant. This is the condition expressed in Eq. 1.

Theorem 1. Assume that Assumptions 1 and 2 are satisfied. For the sequence $\{f^t\}$ generated by BCD, the sequence $\{G(f^t)\}$ converge to G^* and there exists $f^* \in \Pi_{i=1}^N \mathcal{F}_i$ such that

$$G(f^*) = G^* \quad (10)$$

Proof: According to the definition of Eq. (5), in this optimization process, we optimized from the initial parameter $B_{j_k}^{j,k-1}$ to the result $B_{j_k}^{j,k}$, thus establishing the order relation

$$G_{B_{j_k}}(B_{j_k}^{j,k} | f^{j,k-1} \setminus B_{j_k}^{j,k-1}) \leq G_{B_{j_k}}(B_{j_k}^{j,k-1} | f^{j,k-1} \setminus B_{j_k}^{j,k-1})$$

Then we known that function h in Eq. (1) is strictly increasing, it preserve the order relation, then we have

$$G(B_{j_k}^{j,k} | f^{j,k-1} \setminus B_{j_k}^{j,k-1}) \leq G(B_{j_k}^{j,k-1} | f^{j,k-1} \setminus B_{j_k}^{j,k-1})$$

Due to the parameter update rules Line. (10) in Alg. (1), we have the relationship

$$G(f^{j,k}) = G(B_{j_k}^{j,k} | f^{j,k-1} \setminus B_{j_k}^{j,k-1}) \leq G(B_{j_k}^{j,k-1} | f^{j,k-1} \setminus B_{j_k}^{j,k-1}) = G(f^{j,k-1})$$

i.e. each step of updating does not increase the objective value.

Because G has lower bound $G \geq 0$, the non-increasing sequence $G(f^{j,k})$ converges to G^* .

For the sequence $\{f^{j,k}\}$ in closed set $\Pi_{i=1}^N \mathcal{F}_i$, according to Bolzano-Weierstrass theorem, there exists subsequence $\{f^{t_m}\}$ converge to $f^* \in \Pi_{i=1}^N \mathcal{F}_i$ and the subsequence $G(f^{t_m})$ converge to G^* . Then

$$G(f^*) = G^*$$

This completes the proof. \square

Note that Theorem 1 merely demonstrates that the objective function value in the BCD algorithm can converge to a specific value where the objective function is defined. However, under the current assumptions, there are no constraints on the found parameter f^* , which is not necessarily a local optimum and may not even be a stationary point. [54]. The result thus indicates that the BCD algorithm can only partially optimize the calibration problem. Of course, considering practical applications, BCD partially resolve crosstalk phenomena in quantum chips through calibration experiments. [15]

If we wish to determine with certainty whether our calibration optimization results represent at least one stationary point, we need to introduce additional strict assumptions about the objective function.

Assumption 3. (*Stationary point convergence*)

- (*KL property*) The objective function G satisfies the Kurdyka-Łojasiewicz (KL) property on its domain \mathcal{F} .
- (*Unique solution*) Each subproblem in Eq. (5) admits a unique solution, and the objective function strictly decreases with each update.

When Assumption 1 and Assumption 3 are satisfied, the sequence generated by the block coordinate descent algorithm is guaranteed to converge to a stationary point of G [55, 56].

In practice, however, it is impossible to solve the subproblem in Eq. (6) with perfect precision. We terminate the local search after a finite number of iterations, S , which means the solution will inevitably contain some deviation from a true local minimum B_j^* . This inexactness can be bounded, for instance, by the following condition on the obtained solution B_j^S :

$$\|B_j^* - B_j^S\|_\infty < \frac{1}{S} \quad (11)$$

This condition characterizes the result of a single inexact block update. For the overall BCD algorithm, this implies that the sequence of generated parameters is produced by subproblem solutions that are consistently approximate. Therefore, the sequence of solutions $\{B_j^S\}$ obtained throughout the algorithm's execution must satisfy this bound for every block coordinate:

$$\|B_j^* - B_j^S\|_\infty < \frac{1}{S} \quad \forall j = 1, 2, \dots \quad (12)$$

A second, and more critical, challenge arises when the validity condition in Eq. (1) is only approximately satisfied. When this occurs, the global cost function G is no longer guaranteed to be non-increasing at each step, which can impede convergence. There are two primary reasons for this discrepancy. First, random measurement errors are introduced during the process of obtaining function values; the objective function used in optimization is not the ideal G but rather a noisy version $\tilde{G} = G + \text{noise}$. Second, the effects of non-local crosstalk may be neglected if the heuristic model is incomplete, introducing a systematic error even with precise measurements. To investigate the impact of each of these factors separately, we conducted two sets of numerical experiments.

D. Performance of BCD Algorithm

To evaluate the performance and robustness of the BCD algorithm under realistic conditions, we conduct a series of numerical simulations. These simulations are designed to probe the algorithm's sensitivity to three key factors: variations in the underlying physical system, the non-convexity of the optimization landscape, and the presence of experimental noise.

First, the physical parameters that define crosstalk errors can vary significantly between different quantum devices, resulting in different objective functions. To model this diversity, we construct a range of distinct objective functions

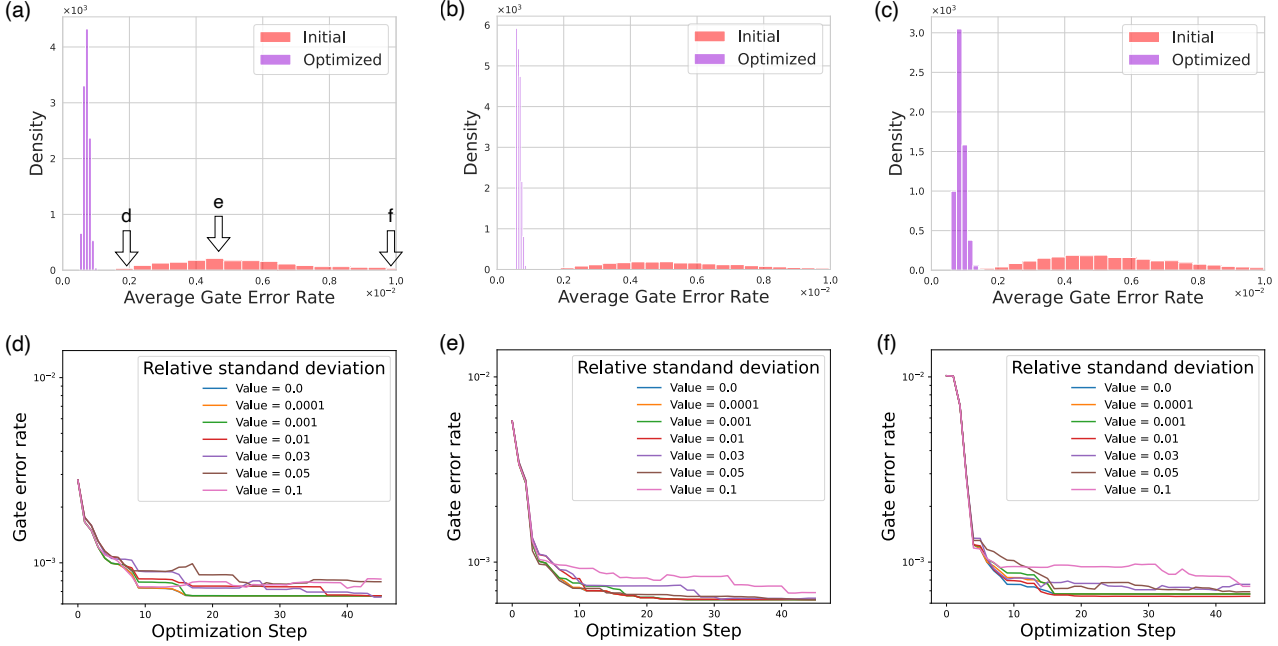


FIG. 2. Optimization performance. (a) We employ probability density functions to describe the distribution of our optimization metric (the average gate error rate) before and after optimization with BCD-NNA, starting from randomly chosen initial points under different error models. (b,c) For a fixed error model, distributions of the average gate error rate before and after optimization when starting from different randomly selected initial points. During optimization in panel (c), the evaluations exhibit a relative standard deviation of 0.2, whereas no such variability is present in panel (b). (d,e,f) Demonstration of the optimization process showing the actual average gate error rate varies with the number of optimization steps starting from different initial points in panel (a). The curves show the actual average gate error rate, while the optimization itself uses evaluations with different relative standard deviations.

by randomly sampling the parameters of the error simulator from within a fixed, physically plausible range. This allows us to assess the general applicability of the algorithm across different hardware instances.

Second, for any given non-convex optimization problem, the algorithm's convergence behavior and final performance can be highly dependent on the choice of the initial point. To investigate this sensitivity, we fix a single error model (i.e., a single objective function) and execute the optimization process from multiple, randomly selected initial parameter settings.

Third, in a real experimental setting, the objective function is not evaluated exactly but is estimated from a finite number of measurements, which introduces stochastic noise. To emulate this, we corrupt the precise values from the error simulator with additive random noise, such that the optimizer operates on these noisy estimates. However, to assess the true quality of the solution, we report the performance using the underlying, noiseless objective function value, which is known within the simulation.

The results of these investigations are summarized in Fig. 2. Under the local-crosstalk assumption, the BCD algorithm consistently improves system performance across all tested error models and from all random initializations. The non-convex nature of the problem is apparent, as different starting points lead to final values of varying quality. Nonetheless, even the worst-performing optimization run achieves a significant improvement over its random initial state. When stochastic measurement noise is introduced, the final performance generally degrades. Interestingly, the noise can occasionally have a beneficial annealing-like effect, enabling the optimizer to escape a shallow local minimum and converge to a superior solution than what might be achieved in a noiseless scenario.

The preceding simulations operated under the assumption that the error model perfectly matched the simulated physical reality (i.e., both contained only local crosstalk). We now consider the more complex case of model mismatch, where the physical system exhibits non-local crosstalk, but the optimization algorithm proceeds with a model that only accounts for local effects. This mismatch introduces a systematic error into the optimization process. As illustrated in Fig. 3, we compare two strategies in this scenario: 1) using a more complex algorithm that correctly models the non-local effects, and 2) using the simpler, misspecified algorithm based on the local crosstalk assumption.

The results show that employing the accurate, more complex model yields significantly better optimization out-

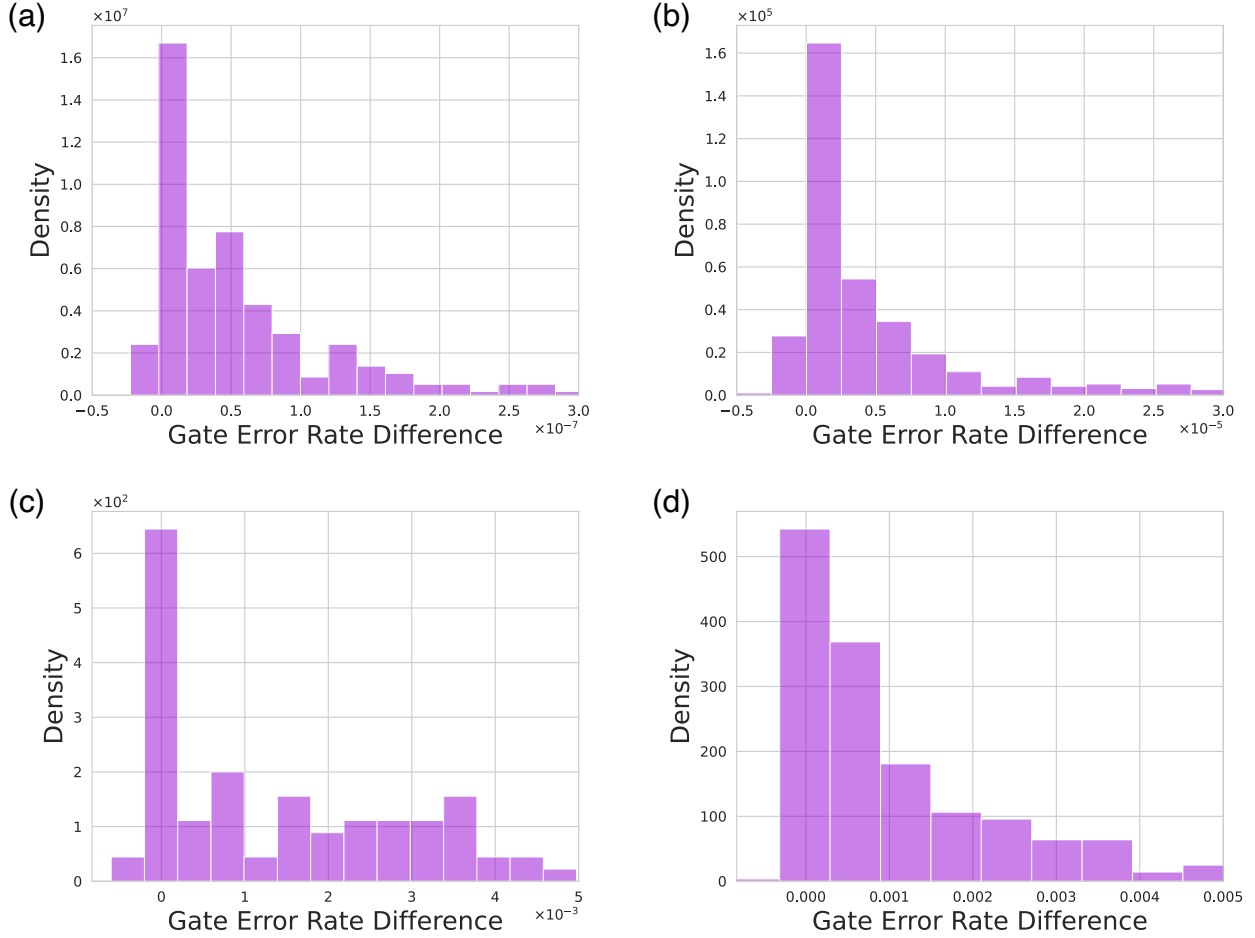


FIG. 3. Impact of nonlocal crosstalk errors on the optimization process In the numerical simulation, we altered the maximum range of random selection for nonlocal crosstalk parameters in the error simulator, incrementally increasing it from (a) to (d), while maintaining the random selection ranges for other local crosstalk parameters unchanged. By repeatedly selecting parameters within their respective ranges to determine the error model, we optimized it using different optimization algorithms. The probability density plots show the distribution of differences in average gate error rates, calculated as the results from crosstalk-unaware optimization minus those from crosstalk-aware optimization.

comes. While the simpler, misspecified model still provides some improvement, its effectiveness is fundamentally limited by the systematic error. This highlights a critical trade-off: the decision to incorporate non-local effects into the optimization model depends on the magnitude of these effects versus the increased complexity and computational cost of the corresponding algorithm.

In summary, the practical application of this optimization framework involves navigating a trade-off between algorithmic stability, computational cost, and ultimate performance, which is dictated by how closely the idealized assumptions are met.

- **Strict Validity and Model Accuracy:** When the crosstalk model is accurate and measurements are precise (approximating the strict satisfaction of the validity condition in Eq. (1)), the algorithm’s stability is assured, and it can reliably converge, as demonstrated in the noiseless cases in Fig. 2. Achieving this in practice requires either a system with negligible unmodeled effects or a significant investment in characterization and computation to build a highly accurate model.
- **Approximate Validity and Practical Constraints:** In practice, the validity condition is often only approximately satisfied due to factors like measurement noise or model mismatch. **Measurement noise**, as shown in Fig. 2, introduces variance and can degrade final performance, although it may occasionally help escape

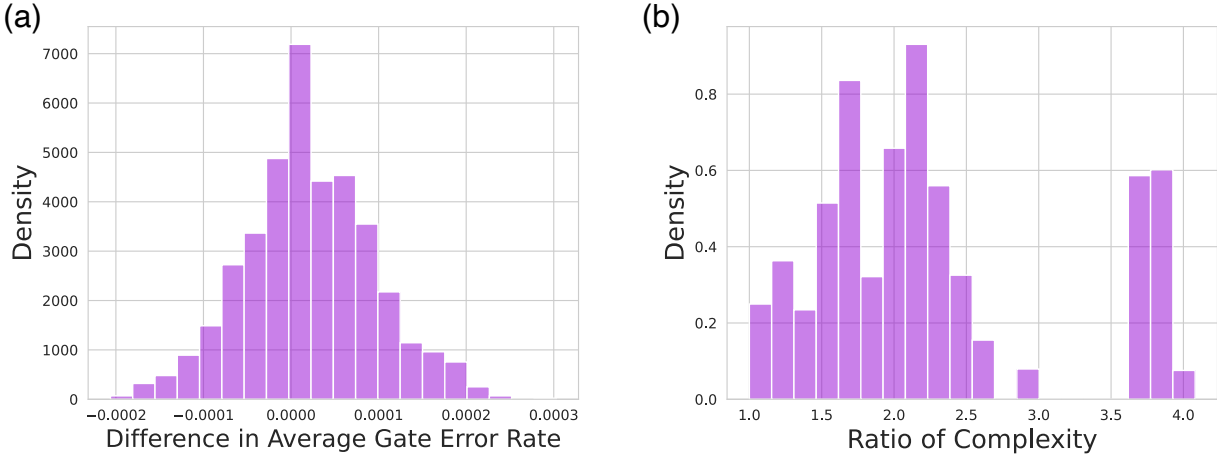


FIG. 4. **NNA for BCD** (a) Probability density plot of the difference in average gate error rate, calculated as BCD-random minus BCD-NNA. (b) Probability density plot of the algorithmic complexity ratio, calculated as BCD-random divided by BCD-NNA, demonstrating markedly lower complexity for BCD-NNA. In both (a) and (b), the optimization algorithms start from random initial points of random error model parameters. The difference between the two optimization algorithms stems solely from the distinct optimization sequences resulting from their parameter block strategies. For each optimization under the same error model parameter, BCD-NNA selects a path derived from the NNA within the strategy subspace, while BCD-random makes random selections within the strategy subspace each time.

local minima. **Model mismatch**, as shown in Fig. 3, imposes a more fundamental limitation on performance. Tolerating this systematic error leads to a simpler, more efficient algorithm but results in a suboptimal solution. Correcting for it improves the outcome at the cost of higher algorithmic complexity.

Ultimately, the choice of strategy depends on the specific requirements of the quantum system, balancing the need for performance against the available resources for characterization and computation.

E. Complexity of BCD

The overall computational complexity of the Block Coordinate Descent (BCD) algorithm can be decomposed into three fundamental components: (1) the number of epochs, in which all parameters are updated once; (2) the number of cost function evaluations, denoted by S_i , that occur within each block during parameter optimization; and (3) the intrinsic computational cost of evaluating each cost function, represented by T_{G_i} . Nevertheless, under identical computational resources allocated per epoch, the performance improvement obtained per epoch typically exhibits a gradually diminishing trend. Hence, from a practical perspective, the total number of epochs is usually fixed to a specific value. Subsequently, the analysis of algorithmic complexity primarily focuses on the variation of the latter two components—namely S_i and T_{G_i} .

In the BCD framework, the set of parameters is partitioned into multiple disjoint blocks, and the parameters within each block are optimized sequentially. The manner in which the parameters are grouped significantly influences the effective search space size, particularly in the presence of crosstalk structures among parameters. For instance, consider a system with $3N$ parameters that are divided into $M = N$ blocks. In this scenario, the average number of parameters contained in each block can be approximated as $|B_i| = 3$, implying that each block spans a three-dimensional search subspace. Assuming that each parameter can be selected from k discrete values, the corresponding search space size for each block is given by:

$$S_i = k^{|B_i|}$$

In contrast, if all parameters are divided into a single block (i.e., $M = 1$), then the BCD algorithm essentially loses its decompositional advantage, and the optimization becomes equivalent to a global search over the entire parameter space. Under such conditions, the dimensionality of the search space is $3N$, and the corresponding search size increases exponentially as k^{3N} .

It is important to note that the BCD algorithm operates in a stepwise optimization manner after the parameters are partitioned into blocks. Each resulting subproblem may still admit simplification by exploiting additional structural properties inherent to the specific problem. To characterize the upper-bound behavior of the algorithm, the complexity associated with a worst-case exhaustive verification is typically employed to estimate the maximum complexity of BCD. However, in practical implementations, strategies such as the *diminishing radius* technique [53] are often introduced to substantially lower the effective search complexity from the naive exponential order of k^n to a reduced order of $\mathcal{O}(3^n)$. Furthermore, various optimization algorithms may be adopted to further accelerate the solution process for each subproblem. It should be emphasized that the choice of specific optimization techniques inevitably leads to variations in the computational complexity. To comprehensively characterize the sub-algorithm complexity S_i , we consider two complementary models:

1. **Empirical complexity model:** $S_i = S \times 3^{|B_i|}$, derived from our numerical implementation using the local search algorithm defined in Eq. (6). This model reflects the practical cost of our specific optimization procedure, where S is the number of iterations and $3^{|B_i|}$ represents the size of the discrete search direction set.
2. **Search-space complexity model:** $S_i = k^{|B_i|}$ where $k \approx 100$, following the theoretical framework established in Ref. [43]. In that work, each subproblem involves optimization over all possible frequency configurations for the gates in the block, yielding a search space of size $k^{|B_i|}$ where k is the number of discrete frequency options per gate (typically $k \sim 10^2$). This model represents the worst-case complexity when exhaustive or grid search is required.

The distinction between these two models has significant implications for evaluating the benefits of ordering optimization. Under the empirical model, which reflects our efficient implementation, the improvement from optimized block ordering is modest (Fig. 5b). However, under the search-space model, which represents the theoretical upper bound applicable to less efficient optimization procedures or exhaustive verification, the improvement becomes substantially larger (Fig. 3e). This observation highlights that the benefits of the proposed SD-TSP formulation scale with the complexity of the underlying sub-algorithm, making it particularly valuable for scenarios where exhaustive or near-exhaustive search is required.

For the theoretical analysis of scaling behavior, we adopt the search-space complexity model $S_i = k^{|B_i|}$ as the representative expression, consistent with the framework of Ref. [43].

After dividing the parameters in the BCD algorithm, it is necessary to consider not only the change of the search space, but also the complexity of obtaining the reduced cost function. It is also necessary to consider the complexity of obtaining the cost objective function. For example, the value of XEB experiment containing $|C_i|$ qubits is used as the reduced cost function. To satisfy Eq. (1), we can find that $|C_i|$ depends on B_i . This process requires multiple calculations of Eq. (13)

$$p_U(x_i) = |\langle x_i | U | 0^{|C_i|} \rangle|^2 \quad (13)$$

If the Feynman path integral method is used, the complexity of the computation increases exponentially with the number of contained qubits $|C_i|$. Also the complexity of the computation increases exponentially with the depth of the circuit, though the depth of the circuit is usually fixed in this problem. Considering also that the total number of measurement samples is S times. The computational complexity is denoted as $S \times t^{|C_i|}$. Since in the process of calculating the XEB of the circuit, the time of classical computation will often be larger than the time of quantum circuit sampling. The complexity of the classical computation is used as the complexity of the reduced objective function. Then the complexity of getting cost function is $T_{G_i} = S \times t^{|C_i|}$

Of course, it is possible to use a more efficient way of calculating XEB or to use other output of the circuit as the reduced cost function, this complexity will be discussed as an example in this paper. If XEB continues to be chosen as the reduced cost function, it is necessary to reduce the number of qubits contained in the circuit as much as possible based on known crosstalk information.

As a result, the complexity of one epoch of BCD algorithm can be obtained as

$$\mathcal{T} = \sum_{i=1}^M \mathcal{T}_i(B_i) = \sum_{i=1}^M S_i \times T_{G_i} = \sum_{i=1}^M S \times k^{|B_i|} t^{|C_i|} \quad (14)$$

Of course, the definition of algorithmic complexity varies depending on the specific optimization algorithms and the choice of different reduced objective function G_i . However, our primary concern lies in how the overall complexity evolves with the increasing number of qubits in the system under the assumption of local crosstalk. This evolution determines whether we can calibrate larger-scale quantum chips. When only local crosstalk exists in the system, with a given upper bound on the block size, the upper bound of function complexity (T_{max}) for each block does not change

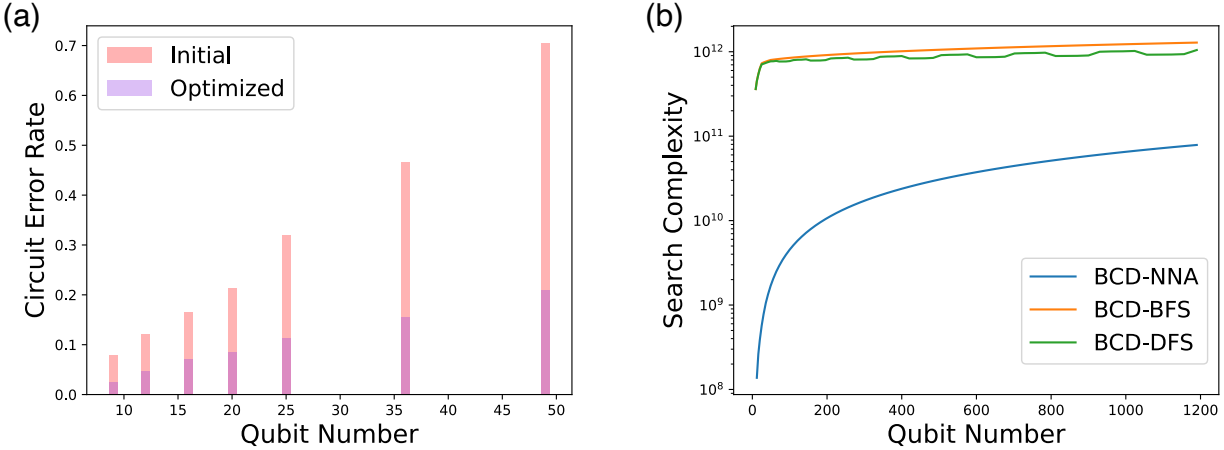


FIG. 5. **Algorithm scaling with increasing number of qubits.** (a) Optimization of quantum chips with varying numbers of qubits using the BCD-NNA algorithm: comparison of circuit error rates before and after optimization. (b) Algorithmic complexity comparison under the search-space complexity model ($S_i = k^{|B_i|}$ with $k = 100$), following the theoretical framework of Ref. [43]. This model represents the worst-case complexity for derivative-free optimization over all frequency configurations. Under this model, BCD-NNA achieves substantial complexity reduction compared to graph-based heuristics (BFS, DFS) employed in the original Snake implementation [15], demonstrating the significant benefit of the SD-TSP formulation for optimizing block order.

with the system size, and at the same time, the upper bound of search space (S_{max}) is also independent of the system size, which means that

$$\mathcal{T} = \sum_{i=1}^M \mathcal{T}_i = \sum_{i=1}^M S_i \times T_{G_i} \leq \sum_{i=1}^M S_{max} \times T_{max} = M \times S_{max} \times T_{max} \quad (15)$$

Here M is related to the total number of block in the system. If parameters are grouped around each qubit, this implies that $M = N$. Therefore, when applying the BCD algorithm for one epoch of parameter optimization, the algorithm's complexity scales with the system size is $\mathcal{O}(N)$.

F. Nearest-neighbor algorithm

In selecting the parameter block strategy for the BCD algorithm, the exponential differences may exist between the complexity of different simplified calibration circuits, so in the process of optimizing different classes of parameters, the complexity of the simplified calibration circuit is an important factor affecting the choice of the BCD algorithm.

When the complexity of the cost function is constant or polynomial with increasing parameters, it has been discussed[57]. Here we focus on when the cost function increases polynomially or exponentially with the increase of the parameters, how should the parameter block strategy be chosen for the BCD algorithm. For superconducting quantum systems, it is clear that when the parameters divided into one block of the qubits are more dispersed, the complexity of obtaining the fidelity of the quantum circuit increases rapidly. Even though the optimization task can be completed in one epoch by such a block strategy, the complexity of this strategy is most likely larger than other strategies. Therefore, the main objective here is to find the BCD algorithm in one epoch with less complexity.

Let $G = (V, E)$ be a complete directed graph, where

$$V = \{1, 2, \dots, n\}$$

is the set of cities, and $E = \{(i, j) \mid i, j \in V, i \neq j\}$ is the set of directed edges representing possible travel between cities.

A path (or Hamiltonian path) in G is an ordering (permutation)

$$\pi = (\pi_1, \pi_2, \dots, \pi_n)$$

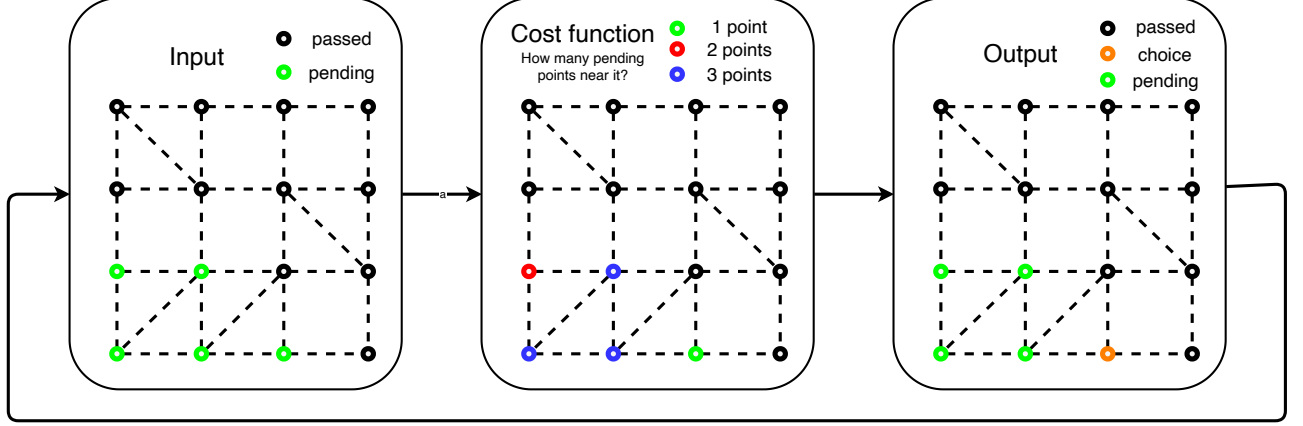


FIG. 6. **Flowchart of the NNA algorithm to solve SD-TSP** Similar to the TSP, but here the cost of the journey is the number of destinations connected to other points that are not passed through. Starting from one seed, the point with the lowest cost among the non-passing points is taken as the destination so that the number of passing points increases. Keep looping until the entire route includes all points. We then use multi-start seeds and select the lowest-cost route.

of all vertices V , which represents the visiting order of the cities by a traveling agent.

Unlike the classical Traveling Salesman Problem (TSP[58–62]), where the cost of traveling from city i to city j is fixed and denoted by $c(i, j)$, in the *Traveling Salesman Problem with Path-Dependent Costs* (TSP-PDC), the cost depends on both the current edge (i, j) and the preceding history of the tour.

Formally, we define the path-dependent cost function as:

$$C : V \times V \times \mathcal{H} \rightarrow \mathbb{R}_{\geq 0}$$

where \mathcal{H} denotes the set of all finite sequences of visited cities (i.e., partial tours), and

$$C(i, j, H)$$

represents the cost of traveling from city i to city j given that the sequence of previously visited cities (the current history) is $H = (v_1, v_2, \dots, v_k)$.

The total cost of a complete tour $\pi = (\pi_1, \pi_2, \dots, \pi_n)$ under a cost function C is then defined recursively as:

$$Cost(\pi; C) = \sum_{t=1}^{n-1} C(\pi_t, \pi_{t+1}, (\pi_1, \pi_2, \dots, \pi_t))$$

The sequence-dependent Traveling Salesman Problem is the combinatorial optimization problem:

$$\min_{\pi} Cost(\pi; C), \quad (16)$$

Note that when $C(i, j, H)$ depends only on (i, j) (that is, $C(i, j, H) = c(i, j)$ for all histories H), the problem reduces to the classical Traveling Salesman Problem(TSP).

In our problem, we usually have another graph $G_p = (V_p, E_p)$, where $V_p = \{1, 2, 3, \dots, N\}$ is the set of qubits and $E_p = \{(i, j) | i, j \in V_p, i \neq j\}$ is the set of two-qubit gate in the chip. To simplify the process of determining how to divide parameters into different blocks initially, we partition the parameters into N blocks. Each block consists of one single-qubit gate parameter and between zero and four two-qubit gate parameters. The number of two-qubit gate parameters in one block depends on whether another single-qubit gate parameter has already been divided. In this case, the position of single-qubit gate parameters and the order in which all single-qubit gate parameters are traversed determine the block set $\mathcal{B} = \{B_j\}_{j=1}^M$. Therefore, the set of qubits and the vertex set in the optimization problem are identical($V_p = V$), while the edge set is typically different($E_p \neq E$). This is because the graph chosen for the TSP problem is complete, with directed edges representing the sequence of parameter block optimizations, allowing edges to exist between any two points. In contrast, the graph is often local due to the positional constraints of the two-qubit gates.

In this TSP formulation, the "travel cost" between two specific blocks is not fixed but depends on the sequence of blocks that the traveler (or qubit) has previously visited. As a result, certain greedy algorithms traditionally used for solving TSP cannot be directly applied. However, the Nearest Neighbor Algorithm (NNA) emerges as a viable alternative in this context [63–66].

Algorithm 2 Nearest-neighbor algorithm

Require: S point set; F cost function

Ensure: R route

```

1:  $k \leftarrow 0$ 
2:  $R_k \leftarrow \emptyset$ ,  $S_k \leftarrow S$ 
3: repeat
4:   choose  $r_k \in \arg \min_{x \in S_k} F(x, S_k, R_k)$ 
5:    $R_{k+1} \leftarrow R_k \cup \{r_k\}$ ,  $S_{k+1} \leftarrow S_k \setminus \{r_k\}$ 
6:    $k \leftarrow k + 1$ 
7: until  $S_k = \emptyset$ 
```

Using the NNA(2) approach, optimization begins with a qubit-centric block. The next step involves identifying the subsequent qubit-centric block with the lowest associated complexity. By iterating this process, a single route for executing the Block Coordinate Descent (BCD) algorithm can be determined. As shown in Fig. (II F), since the cost function in practical problems is difficult to express intuitively, the cost is defined here as the number of points not visited around the target point to demonstrate the NNA algorithm. If the algorithm is initiated from each qubit in turn, N different routes are generated, and it becomes straightforward to select the route that minimizes the overall time. Although NNA is inherently a greedy algorithm, it provides an efficient means to identify the desired route in polynomial time.

Here, we aim to examine the impact of the NNA algorithm on the BCD algorithm with numerical simulation. First, we considered the differences arising from various block strategies within the BCD algorithm. These differences primarily manifest in two aspects: optimization results and optimization complexity. We randomly select block strategies from the permissible strategy space and compare them with those chosen by the NNA algorithm. As shown in Fig. (4), there is no significant difference between the optimization results of randomly selected block strategy and specific strategy provided by NNA for different error models. However, there is a significant difference in the optimization complexity of the two strategies, especially when the number of qubits increases. This means that specific strategy provided by NNA can achieve optimization in a shorter time with similar optimization results.

Given the improvements of the NNA algorithm over the BCD algorithm, we are increasingly interested in how the optimization algorithm performs as quantum chips incorporate more qubits, and whether the complexity reduction achieved by the NNA algorithm changes as the number of qubits increases. As shown in Fig. (5), the optimization algorithm continues to effectively reduce the error rate of quantum circuits as the number of qubits in the system increases. Simultaneously, the impact of the NNA algorithm on computational complexity becomes more pronounced as the number of qubits grows.

The algorithm described above requires only information about the presence of crosstalk in the system, while the specific strength of the crosstalk is not a necessary input. Detecting the strength of crosstalk becomes relevant only under particular circumstances. Specifically, if the system exhibits neither exceptionally strong nor unexpectedly weak crosstalk, measuring the crosstalk strength does not yield significant improvements in the BCD algorithm.

However, if certain crosstalk interactions are found to be unusually strong, additional experimental methods can be used to mitigate these effects. Simultaneously, it becomes beneficial to group the parameters influenced by these strong crosstalk interactions into fewer blocks. By confining the influence of crosstalk within the parameters of a single block, the crosstalk between blocks is effectively reduced. Nevertheless, this approach increases the size of each block ($|B_j|$) and the associated coupling terms ($|C_j|$), thereby leading to a rise in the overall computational complexity.

Conversely, if certain crosstalk interactions are found to be exceptionally weak, the inclusion range of the reduced objective function G_{B_j} can be narrowed, which decreases $|C_j|$ and subsequently reduces the computational complexity of the BCD algorithm. In cases where a large number of weak crosstalk interactions are present, such that the qubit system can be divided into two or more independent subsystems with negligible mutual influence, the original N -qubit system can be partitioned into smaller subsystems. Given the exponential increase in the complexity of Eq. (2) with the number of qubits, this partitioning significantly reduces computational complexity. Furthermore, the smaller subsystems can be processed in parallel using the BCD algorithm, further reducing the computational burden.

III. CONCLUSION

As quantum computers remain in the Noisy Intermediate-Scale Quantum (NISQ) era, it is still essential to leverage classical computing resources to assist in the benchmarking and calibration processes. Classical computers play a critical role in evaluating the performance of quantum processors by quantifying the gap between the realized quantum circuit and the idealized circuit implementation. In this work, we have established the mathematical equivalence between the Snake optimizer and Block Coordinate Descent (BCD), providing a rigorous theoretical foundation for this widely-used calibration strategy. This formalization enables the application of classical optimization theory to analyze convergence properties and complexity scaling. Building on this foundation, we formulate the block ordering problem as a Sequence-Dependent Traveling Salesman Problem (SD-TSP) and solve it efficiently using the Nearest Neighbor Algorithm (NNA), achieving systematic complexity reduction compared to the graph-based heuristics (BFS, DFS) employed in the original Snake implementation.

The proposed method achieves a computational complexity of $O(N)$ under the assumption of local crosstalk, making it highly efficient for practical scenarios. Furthermore, the approach demonstrates strong robustness against random noise, ensuring reliable performance in realistic, noisy quantum environments. However, the method's performance can deteriorate in the presence of strong nonlocal crosstalk interactions, which underscores the limitations of the current algorithm and the need for further refinements.

To address these challenges, future research will focus on the development of advanced optimization techniques. Specifically, adaptive crosstalk detection mechanisms will be explored to dynamically identify and mitigate the effects of nonlocal crosstalk. Additionally, parallel optimization strategies will be incorporated to enhance the scalability of the algorithm, enabling it to handle larger quantum systems more effectively. These advancements aim to bridge the gap between theoretical models and practical implementations, further improving the calibration and benchmarking of quantum processors in the NISQ era.

ACKNOWLEDGMENTS

This work is supported by Shanghai Municipal Science and Technology (Grant No. 25LZ2600200), National Natural Science Foundation of China (Grants No. 92365111), Beijing Natural Science Foundation (Grants No. Z220002), and the Innovation Program for Quantum Science and Technology (Grant No. 2021ZD0302400).

[1] P. W. Shor, Polynomial-time algorithms for prime factorization and discrete logarithms on a quantum computer, [SIAM Journal on Computing](#) **26**, 1484 (1997).

[2] Y. Cao, J. Romero, J. P. Olson, M. Degroote, P. D. Johnson, M. Kieferova, I. D. Kivlichan, T. Menke, B. Peropadre, N. P. D. Sawaya, S. Sim, L. Veis, and A. Aspuru-Guzik, Quantum chemistry in the age of quantum computing, [CHEMICAL REVIEWS](#) **119**, 10856 (2019).

[3] B. Bauer, S. Bravyi, M. Motta, and G. K.-L. Chan, Quantum algorithms for quantum chemistry and quantum materials science, [CHEMICAL REVIEWS](#) **120**, 12685 (2020).

[4] S. McArdle, S. Endo, A. Aspuru-Guzik, S. Benjamin, and X. Yuan, Quantum computational chemistry, [REVIEWS OF MODERN PHYSICS](#) **92**, 10.1103/RevModPhys.92.015003 (2020).

[5] M. Cerezo, A. Arrasmith, R. Babbush, S. C. Benjamin, S. Endo, K. Fujii, J. R. McClean, K. Mitarai, X. Yuan, L. Cincio, and P. J. Coles, Variational quantum algorithms, [NATURE REVIEWS PHYSICS](#) **3**, 625 (2021).

[6] J. Tilly, H. Chen, S. Cao, D. Picozzi, K. Setia, Y. Li, E. Grant, L. Wossnig, I. Rungger, G. H. Booth, and J. Tennyson, The variational quantum eigensolver: A review of methods and best practices, [PHYSICS REPORTS-REVIEW SECTION OF PHYSICS LETTERS](#) **986**, 1 (2022).

[7] A. Di Meglio, K. Jansen, I. Tavernelli, C. Alexandrou, S. Arunachalam, C. W. Bauer, K. Borras, S. Carrazza, A. Crippa, V. Croft, R. de Putter, A. Delgado, *et al.*, Quantum computing for high-energy physics: State of the art and challenges, [PRX QUANTUM](#) **5**, 10.1103/PRXQuantum.5.037001 (2024).

[8] B. Fauseweh, Quantum many-body simulations on digital quantum computers: State-of-the-art and future challenges, [NATURE COMMUNICATIONS](#) **15**, 10.1038/s41467-024-46402-9 (2024).

[9] D. Pan, G.-L. Long, L. Yin, Y.-B. Sheng, D. Ruan, S. X. Ng, J. Lu, and L. Hanzo, The evolution of quantum secure direct communication: On the road to the qinternet, [IEEE COMMUNICATIONS SURVEYS AND TUTORIALS](#) **26**, 1898 (2024).

[10] R. Santagati, A. Aspuru-Guzik, R. Babbush, M. Degroote, L. Gonzalez, E. Kyoseva, N. Moll, M. Oppel, R. M. Parrish, *et al.*, Drug design on quantum computers, [NATURE PHYSICS](#) **20**, 549 (2024).

[11] F. Arute, K. Arya, R. Babbush, D. Bacon, J. C. Bardin, R. Barends, R. Biswas, S. Boixo, *et al.*, Quantum supremacy using a programmable superconducting processor, [Nature](#) **574**, 505 (2019).

- [12] M. Gong, S. Wang, C. Zha, M.-C. Chen, H.-L. Huang, Y. Wu, Q. Zhu, Y. Zhao, S. Li, S. Guo, H. Qian, *et al.*, Quantum walks on a programmable two-dimensional 62-qubit superconducting processor, *Science* **372**, 948 (2021).
- [13] Y. Wu, W.-S. Bao, S. Cao, F. Chen, M.-C. Chen, X. Chen, T.-H. Chung, H. Deng, Y. Du, D. Fan, M. Gong, C. Guo, *et al.*, Strong quantum computational advantage using a superconducting quantum processor, *Physical Review Letters* **127**, 180501 (2021), pRL.
- [14] Q. Zhu, S. Cao, F. Chen, M.-C. Chen, X. Chen, T.-H. Chung, H. Deng, Y. Du, D. Fan, M. Gong, C. Guo, C. Guo, S. Guo, L. Han, L. Hong, H.-L. Huang, *et al.*, Quantum computational advantage via 60-qubit 24-cycle random circuit sampling, *Science Bulletin* **67**, 240 (2022).
- [15] P. V. Klimov, A. Bengtsson, C. Quintana, A. Bourassa, S. Hong, A. Dunsworth, K. J. Satzinger, W. P. Livingston, V. Sivak, *et al.*, Optimizing quantum gates towards the scale of logical qubits, *Nature Communications* **15**, 2442 (2024).
- [16] R. Acharya, D. A. Abanin, L. Aghababaie-Beni, I. Aleiner, T. I. Andersen, M. Ansmann, F. Arute, K. Arya, A. Asfaw, N. Astrakhantsev, J. Atalaya, *et al.*, Quantum error correction below the surface code threshold, *Nature* **638**, 920 (2025).
- [17] D. Gao, D. Fan, C. Zha, J. Bei, G. Cai, J. Cai, S. Cao, F. Chen, J. Chen, K. Chen, X. Chen, *et al.*, Establishing a new benchmark in quantum computational advantage with 105-qubit zuchongzhi 3.0 processor, *Physical Review Letters* **134**, 090601 (2025), pRL.
- [18] Z. Chen, W. Liu, Y. Ma, W. Sun, R. Wang, H. Wang, H. Xu, G. Xue, H. Yan, Z. Yang, J. Ding, Y. Gao, F. Li, Y. Zhang, Z. Zhang, Y. Jin, H. Yu, J. Chen, and F. Yan, Efficient implementation of arbitrary two-qubit gates using unified control, *Nature Physics* **21**, 1489 (2025).
- [19] J. Preskill, Quantum computing in the nisq era and beyond, *QUANTUM* **2**, 10.22331/q-2018-08-06-79 (2018).
- [20] S. Endo, Z. Cai, S. C. Benjamin, and X. Yuan, Hybrid quantum-classical algorithms and quantum error mitigation, *JOURNAL OF THE PHYSICAL SOCIETY OF JAPAN* **90**, 10.7566/JPSJ.90.032001 (2021).
- [21] G. P. Fedorov and A. V. Ustinov, Automated analysis of single-tone spectroscopic data for cqed systems, *Quantum Science and Technology* **4**, 045009 (2019).
- [22] M. Kliesch and I. Roth, Theory of quantum system certification, *PRX Quantum* **2**, 010201 (2021).
- [23] Y. Gu, W.-F. Zhuang, X. Chai, and D. E. Liu, Benchmarking universal quantum gates via channel spectrum, *Nature Communications* **14**, 5880 (2023).
- [24] E. Magesan, J. M. Gambetta, B. R. Johnson, C. A. Ryan, J. M. Chow, S. T. Merkel, M. P. da Silva, G. A. Keefe, M. B. Rothwell, T. A. Ohki, M. B. Ketchen, and M. Steffen, Efficient measurement of quantum gate error by interleaved randomized benchmarking, *Physical Review Letters* **109**, 080505 (2012).
- [25] S. Boixo, S. V. Isakov, V. N. Smelyanskiy, R. Babbush, N. Ding, Z. Jiang, M. J. Bremner, J. M. Martinis, and H. Neven, Characterizing quantum supremacy in near-term devices, *Nature Physics* **14**, 595 (2018).
- [26] A. Erhard, J. J. Wallman, L. Postler, M. Meth, R. Stricker, E. A. Martinez, P. Schindler, T. Monz, J. Emerson, and R. Blatt, Characterizing large-scale quantum computers via cycle benchmarking, *Nature Communications* **10**, 5347 (2019).
- [27] J. Helsen, X. Xue, L. M. K. Vandersypen, and S. Wehner, A new class of efficient randomized benchmarking protocols, *npj Quantum Information* **5**, 71 (2019).
- [28] T. J. Proctor, A. Carignan-Dugas, K. Rudinger, E. Nielsen, R. Blume-Kohout, and K. Young, Direct randomized benchmarking for multiqubit devices, *Physical Review Letters* **123**, 030503 (2019).
- [29] J. Eisert, D. Hangleiter, N. Walk, I. Roth, D. Markham, R. Parekh, U. Chabaud, and E. Kashefi, Quantum certification and benchmarking, *Nature Reviews Physics* **2**, 382 (2020).
- [30] S. Resch and U. R. Karpuzcu, Benchmarking quantum computers and the impact of quantum noise, *ACM Comput. Surv.* **54**, Article 142 (2021).
- [31] J. Helsen, I. Roth, E. Onorati, A. H. Werner, and J. Eisert, General framework for randomized benchmarking, *PRX Quantum* **3**, 020357 (2022).
- [32] T. Proctor, K. Rudinger, K. Young, E. Nielsen, and R. Blume-Kohout, Measuring the capabilities of quantum computers, *Nature Physics* **18**, 75 (2022).
- [33] T. Proctor, K. Young, A. D. Baczewski, and R. Blume-Kohout, Benchmarking quantum computers, *Nature Reviews Physics* **7**, 105 (2025).
- [34] E. Knill, D. Leibfried, R. Reichle, J. Britton, R. B. Blakestad, J. D. Jost, C. Langer, R. Ozeri, S. Seidelin, and D. J. Wineland, Randomized benchmarking of quantum gates, *Physical Review A* **77**, 012307 (2008).
- [35] M. Bal, A. A. Murthy, S. Zhu, F. Crisa, X. You, Z. Huang, T. Roy, J. Lee, D. v. Zanten, *et al.*, Systematic improvements in transmon qubit coherence enabled by niobium surface encapsulation, *NPJ QUANTUM INFORMATION* **10**, 10.1038/s41534-024-00840-x (2024).
- [36] C. Wang, X. Li, H. Xu, Z. Li, J. Wang, Z. Yang, Z. Mi, X. Liang, T. Su, C. Yang, G. Wang, W. Wang, Y. Li, *et al.*, Towards practical quantum computers: transmon qubit with a lifetime approaching 0.5 milliseconds, *NPJ QUANTUM INFORMATION* **8**, 10.1038/s41534-021-00510-2 (2022).
- [37] A. P. M. Place, L. V. H. Rodgers, P. Mundada, B. M. Smitham, M. Fitzpatrick, Z. Leng, A. Premkumar, J. Bryon, A. Vrajitoarea, *et al.*, New material platform for superconducting transmon qubits with coherence times exceeding 0.3 milliseconds, *NATURE COMMUNICATIONS* **12**, 10.1038/s41467-021-22030-5 (2021).
- [38] J. J. Burnett, A. Bengtsson, M. Scigliuzzo, D. Niegpc, M. Kudra, P. Delsing, and J. Bylander, Decoherence benchmarking of superconducting qubits, *NPJ QUANTUM INFORMATION* **5**, 10.1038/s41534-019-0168-5 (2019).
- [39] M. A. Rol, L. Ciorciaro, F. K. Malinowski, B. M. Tarasinski, R. E. Sagastizabal, C. C. Bultink, Y. Salathe, N. Haandbaek, J. Sedivy, and L. DiCarlo, Time-domain characterization and correction of on-chip distortion of control pulses in a quantum processor, *Applied Physics Letters* **116**, 054001 (2020).
- [40] P. Krantz, M. Kjaergaard, F. Yan, T. P. Orlando, S. Gustavsson, and W. D. Oliver, A quantum engineer's guide to

superconducting qubits, *Applied Physics Reviews* **6**, 021318 (2019).

[41] J. Koch, T. M. Yu, J. Gambetta, A. A. Houck, D. I. Schuster, J. Majer, A. Blais, M. H. Devoret, S. M. Girvin, and R. J. Schoelkopf, Charge-insensitive qubit design derived from the cooper pair box, *Physical Review A* **76**, 042319 (2007).

[42] H. Ai and Y.-x. Liu, Scalable parameter design for superconducting quantum circuits with graph neural networks, *Physical Review Letters* **135**, 040601 (2025), pRL.

[43] P. Klimov, J. Kelly, J. M. Martinis, and H. Neven, The snake optimizer for learning quantum processor control parameters, *ArXiv* **abs/2006.04594** (2020).

[44] Y. Arjevani, Y. Carmon, J. C. Duchi, D. J. Foster, N. Srebro, and B. Woodworth, Lower bounds for non-convex stochastic optimization, *Mathematical Programming* **199**, 165 (2023).

[45] S. Ghadimi and G. Lan, Stochastic first- and zeroth-order methods for nonconvex stochastic programming, *SIAM Journal on Optimization* **23**, 2341 (2013).

[46] Y. Nesterov, A. Gasnikov, S. Guminov, and P. Dvurechensky, Primal-dual accelerated gradient methods with small-dimensional relaxation oracle, *arXiv e-prints* , *arXiv:1809.05895* (2018).

[47] A. Khaled and P. Richtárik, Better theory for sgd in the nonconvex world, *arXiv e-prints* , *arXiv:2002.03329* (2020).

[48] K. A. Sankararaman, S. De, Z. Xu, W. Ronny Huang, and T. Goldstein, The impact of neural network overparameterization on gradient confusion and stochastic gradient descent, *arXiv e-prints* , *arXiv:1904.06963* (2019).

[49] M. Schmidt, N. Le Roux, and F. Bach, Minimizing finite sums with the stochastic average gradient, *arXiv e-prints* , *arXiv:1309.2388* (2013).

[50] A. Agarwal, P. L. Bartlett, P. Ravikumar, and M. J. Wainwright, Information-theoretic lower bounds on the oracle complexity of stochastic convex optimization, *IEEE Transactions on Information Theory* **58**, 3235 (2012).

[51] M. Razaviyayn, M. Hong, and Z. Q. Luo, A unified convergence analysis of block successive minimization methods for nonsmooth optimization, *SIAM JOURNAL ON OPTIMIZATION* **23**, 1126 (2013).

[52] B. Woodworth and N. Srebro, Tight complexity bounds for optimizing composite objectives (2016).

[53] H. Lyu, Convergence and complexity of block coordinate descent with diminishing radius for nonconvex optimization, *arXiv e-prints* , *arXiv:2012.03503* (2020).

[54] M. J. D. Powell, On search directions for minimization algorithms, *Mathematical Programming* **4**, 193 (1973).

[55] P. Tseng, Convergence of a block coordinate descent method for nondifferentiable minimization, *Journal of Optimization Theory and Applications* **109**, 475 (2001).

[56] H. Attouch, J. Bolte, and B. F. Svaiter, Convergence of descent methods for semi-algebraic and tame problems: proximal algorithms, forwardâ€¢backward splitting, and regularized gaussâ€¢seidel methods, *Mathematical Programming* **137**, 91 (2013).

[57] J. Nutini, I. Laradji, and M. Schmidt, Let's make block coordinate descent converge faster: Faster greedy rules, message-passing, active-set complexity, and superlinear convergence, *arXiv e-prints* , *arXiv:1712.08859* (2017).

[58] M. Held and R. M. Karp, *A dynamic programming approach to sequencing problems* (1961).

[59] S. Lin, Computer solutions of the traveling salesman problem, *The Bell System Technical Journal* **44**, 2245 (1965).

[60] M. Dorigo and L. M. Gambardella, Ant colonies for the travelling salesman problem, *Biosystems* **43**, 73 (1997).

[61] K. Helsgaun, An effective implementation of the linâ€¢kernighan traveling salesman heuristic, *European Journal of Operational Research* **126**, 106 (2000).

[62] C. Rego, D. Gamboa, F. Glover, and C. Osterman, Traveling salesman problem heuristics: Leading methods, implementations and latest advances, *European Journal of Operational Research* **211**, 427 (2011).

[63] D. J. Rosenkrantz, R. E. Stearns, and P. M. Lewis, Approximate algorithms for the traveling salesperson problem, in *15th Annual Symposium on Switching and Automata Theory (swat 1974)* (1974) pp. 33â€¢42.

[64] D. S. Johnson, Local optimization and the traveling salesman problem, in *Automata, Languages and Programming*, edited by M. S. Paterson (Springer Berlin Heidelberg) pp. 446â€¢461.

[65] O. Pedro, R. Saldanha, and R. Camargo, A tabu search approach for the prize collecting traveling salesman problem, *Electronic Notes in Discrete Mathematics* **41**, 261 (2013).

[66] P. Hansen and N. Mladenović, Variable neighborhood search, in *Handbook of Heuristics*, edited by R. Martí, P. M. Pardalos, and M. G. C. Resende (Springer International Publishing, Cham, 2018) pp. 759â€¢787.